Three-dimensional chiral Veselago lensing

S. Tchoumakov,[1,][*] J. Cayssol,[2] and A. G. Grushin [1]

[1]*Université Grenoble Alpes, CNRS, Grenoble INP, Institut Néel, F-38000 Grenoble, France*
[2]*Université Bordeaux, CNRS, LOMA, UMR 5798, F-33405 Talence, France*

The effect by which light focuses upon entering a medium with a negative refractive index, known as Veselago lensing, may enable optical imaging below the diffraction limit. Similarly, focusing electrons across a *p-n* junction could realize a technologically promising electronic Veselago lens. However, its scope remains limited by the lack of three-dimensional platforms and its insensitivity to computational degrees of freedom, such as spin or chirality. Here, we propose a single-material three-dimensional electronic Veselago lens that selectively focuses electrons of a given chirality. Using the chiral anomaly of topological semimetals it is possible to create a sharp *p-n* junction for a single chirality, a chiral Veselago lens, and tune it with a magnetic field to an ideal lensing condition. We estimate that chiral Veselago lensing is observable in nonlocal transport and spectroscopy experiments. In particular, we show that the chiral Veselago lens leads to giant nonlocal magnetoresistance.

I. INTRODUCTION

The similarities between the light-ray construction in optics and the semiclassical trajectories of electrons [1,2] host the potential for new applications in electronics, such as electronic lenses, interferometers, or beam splitters at the micrometer scale [3–5]. To reach this potential, controlling the involved material interfaces is crucial. In optics, the trajectory of light is deflected at the interface between two media, allowing one to focus, guide, and disperse light controllably. In particular, between media with opposite handedness, where the optical index changes sign, lensing can occur even for a flat interface, a phenomenon coined Veselago lensing [6]. In electronics, a *p-n* junction can act as an electronic Veselago lens by focusing two-dimensional (2D) electrons with pseudorelativistic, linear band dispersion [3,7–12], an effect that has only been realized in graphene [13–16].

The prospect of creating useful devices based on electronic Veselago lenses faces three fundamental problems. The first problem is that we lack a three-dimensional (3D) Veselago lens. Theoretically, a *p-n* junction sharper than the Fermi wavelength based on 3D relativistic metals, such as Weyl or Dirac metals [17], can Veselago-lens [7,12], in analogy with graphene. While bulk 3D metals have the advantage of a larger carrier density, this property is also a drawback as they are not easily gated. The second problem is creating a clean interface. A *p-n* junction created via chemical doping or by interfacing *p*-doped and *n*-doped samples will likely be disordered by impurities or lattice mismatch. The interface could accumulate charge, affecting electronic transport in undesirable ways [18]. The last problem is that any proposed or realized electronic Veselago lens seems insensitive to computational degrees of freedom, such as spin or chirality. These three problems materialize in the challenge to realize

a single-material 3D Veselago lens that could select specific electronic degrees of freedom.

In this paper we take a significant step to solve these problems by proposing how to Veselago-lens a single chirality of 3D Weyl quasiparticles controllably. The chirality is a quantum mechanical degree of freedom of 3D Weyl quasiparticles, labeled by $\pm$ depending on whether the spin is aligned or antialigned with the electron's momentum, which can be used for computation [19]. By locally activating the chiral anomaly, an effect that overpopulates one chirality with respect to the other in the presence of collinear electric and magnetic fields, it is possible to create a sharp *p-n* junction for a single chirality. The resulting chiral Veselago lensing can be detected either by spectroscopic probes, such as scanning tunneling microscopy (STM), or nonlocal transport.

Because of the chiral anomaly, the lensing can be tuned with electric and magnetic fields to modulate the intensity of the image charge in STM or the image current in nonlocal transport. We also show that ordinary, quadratically dispersing electrons can Veselago-lens stronger than Weyl electrons, albeit without the degree of control offered by the chiral anomaly and suffering from a charging layer at the *p-n* interface. Therefore the chiral anomaly, unique to Weyl semimetals, is the optimal tool to realize a clean 3D chiral Veselago lens.

II. MODEL

Weyl semimetals host pairs of linearly dispersing bands separated in momentum space, known as Weyl cones. Each cone can be described by the Hamiltonian

$$\hat{H}_W = (v_F \mathbf{k} - \mathbf{b}) \cdot \hat{\boldsymbol{\sigma}} - \mu, \tag{1}$$

where $\boldsymbol{\sigma}$ is a vector of Pauli matrices, μ is the chemical potential, v_F is the Fermi velocity, and $\mathbf{b}$ determines the momentum space separation between Weyl cones. The eigenstates of $\hat{H}_W$ depend on the sign of v_F, which defines the chirality
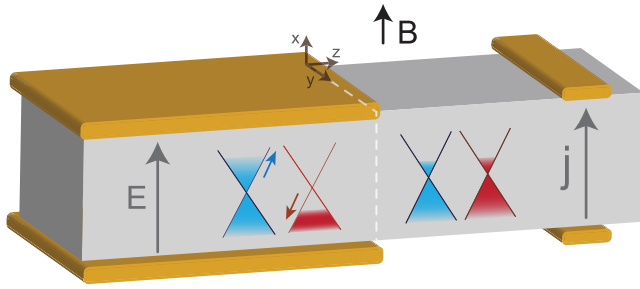
*serguei.tchoumakov@neel.cnrs.fr

FIG. 1. Chiral Veselago lens based on the chiral anomaly. A uniform magnetic field **B** is applied to a Weyl semimetal, while the electric field **E** is only applied for $z < 0$, with two metallic gates (left orange/gold gates). This configuration generates a charge imbalance between Weyl quasiparticles of opposite chiralities (red and blue cones) for $z < 0$ due to the chiral anomaly, while maintaining the total charge constant. This creates an ideal *p-n* junction for a single chirality (blue cones), that Veselago-lenses a measurable nonlocal current at $z > 0$, tuned by changing **B**, and measured by narrow electrodes (in orange/gold at right).

$\mathrm{sgn}(v_F) = \chi = \pm$. Weyl cones come in pairs of opposite χ and, in certain materials, they can be tilted [20] or anisotropic [17]. Here, we focus on materials where these effects are negligible, as discussed at the end.

In the presence of electric (**E**) and magnetic (**B**) fields, the transport of Weyl quasiparticles depends on their respective chirality, as reflected by the continuity equations

$$\frac{\partial n_\chi}{\partial t} + \nabla \cdot \mathbf{j}_\chi = \chi \frac{e^2}{2\pi^2 \hbar^2} \mathbf{E} \cdot \mathbf{B}, \qquad (2)$$

where $n_\pm$ and $\mathbf{j}_\pm$ are, respectively, the charge and current distributions of carriers with $\chi = \pm$. The source term on the right-hand side creates an imbalance Δn between the chiral charges n_+ and n_-, without altering the total charge $n = n_+ + n_-$. This term, known as the chiral anomaly, is responsible for anomalous transport responses, such as the enhancement of the magnetoconductance of Weyl semimetals [17,21].

The chiral anomaly competes with intervalley scattering, leading to a charge imbalance between Weyl nodes with opposite chiralities in the steady state. The intervalley scattering time τ can range from a picosecond in TaAs to a nanosecond in Na$_3$Bi [22,23]. The chiral charge imbalance $\Delta n = n_+ - n_- = \frac{\tau e^2}{2\pi^2 \hbar^2} \mathbf{E} \cdot \mathbf{B}$ equals the carrier density n for a magnetic field $B_c \equiv 2\mu^3/(3v^3 e^2 \tau E)$. For $n = 10^{21}$ cm^{-3}, $\tau = 10^{-9}$ s [22–24], and $E \approx 10^6$ V m^{-1}, this crossover field is $B_c = 1$ T. Beyond B_c, the chiral anomaly reverses the type of carriers of one of the Weyl nodes, e.g., from electrons to holes. Hence, if $B > B_c$ is applied homogeneously and the E is not homogeneous, e.g., stepwise as illustrated in Fig. 1, the chiral anomaly creates an effective *p-n* junction for a single Weyl chirality.

The main goal of this paper is to explain how to realize and detect a single-chirality Veselago lens, under the above conditions. To this end, we discuss spectroscopy and nonlocal transport responses of a single Weyl cone to determine the ideal conditions for single-chirality Veselago lensing. Combining the contributions from the two chiralities we discuss how chiral Veselago lensing can be detected using the simple setup in Fig. 1. In the Supplemental Material [25] we propose

two related, albeit less practical, devices to detect directly chiral Veselago lensing in spectroscopy and in nonlocal transport.

We model the change in the carrier density with a stepwise chemical potential, where $\mu_L = (\mu^3 \pm \frac{3}{2} v^3 e^2 \tau \mathbf{E} \cdot \mathbf{B})^{1/3}$ for $z < 0$ [23] and $\mu_R = \mu$ for $z > 0$ (*L* and *R* denote left and right of the interface, respectively).

III. CHARGE DISTRIBUTION IN A CHIRAL VESELAGO LENS

To visualize and understand the ideal conditions for Veselago lensing, we calculate the charge distribution created by a local potential due to an impurity, or the tip of a STM. For a local potential $V(\mathbf{r}) = \delta(\mathbf{r}_\parallel)\delta(z - z_0)\delta V$ there is a redistribution of charge $\delta n(z) = \Pi(z, z_0)\delta V$ that depends on the polarizability [26]

$$\Pi(z, z') = -\frac{1}{2\pi} \int d\omega \, \mathrm{Tr}\big[\hat{G}(z, z')\hat{G}(z', z)\big], \qquad (3)$$

written in terms of the Green's function $\hat{G}(z, z')$, where we account for scattering with a mean free path $\ell \gg 1/k_F$ (see Supplemental Material [25] for details).

In Figs. 2(b) and 2(c) we plot the polarizability as a function of the x and z coordinates. The coordinates are given in units of $1/k_F$, and the polarizability in units of $\mu_L N_0$, with $N_0 = k_F^3/(2\pi^2 \mu_L)$ being the density of states at $z < 0$, where the impurity is located. We compare the case of a single Weyl chirality with a 3D electron gas, with a quadratic band structure [25]. In a *n-n* (or *p-p*) junction, the charge distribution shows the usual Friedel oscillations on both sides of the junction [see Fig. 2(b)]. The period is different on both sides due to the change in the Fermi wave vector when crossing the interface [26].

The main difference between the *n-n* junction in Fig. 2(b) and the *p-n* junction in Fig. 2(c) is the appearance of an image charge as a consequence of Veselago lensing. Veselago lensing occurs because the in-plane group velocity changes sign across the interface, $\mathbf{v}_L = -\mathbf{v}_R$, due to the conservation of the in-plane wave vector $\mathbf{k}_\parallel$. This condition can be met for both a 3D electron gas and a Weyl semimetal *p-n* junction, but the intensity of the image charge is larger for the former than the latter due to the slower decay of Friedel oscillations in a normal electron gas [27–30].

However, a drawback of using a 3D electron gas is that the electron density across the *p-n* junction is not constant, and one should expect a built-in interface potential over a finite distance d. When $k_F d \gg 1$, we find [25] that the amplitude of the Veselago image rapidly decays [14]. For typical 3D metals $d > 10$ μm, so $k_F d \gg 1$ [31], implying that the corresponding image charge is unobservable in practice [14]. In contrast, in the chiral Veselago lens in Fig. 1 the total charge remains constant, and charges are only transferred between cones of opposite chirality. The electric field extends beyond the parallel plates on a distance of the order of the distance between the two plates, so we can expect a sharp interface potential for thin film samples.

So far we have assumed symmetric *p-n* junctions, i.e., those where k_F is equal on both sides of the interface. Deviations from this condition blur and change the location of the image charge [25]. Reaching ideal lensing is unrealistic with
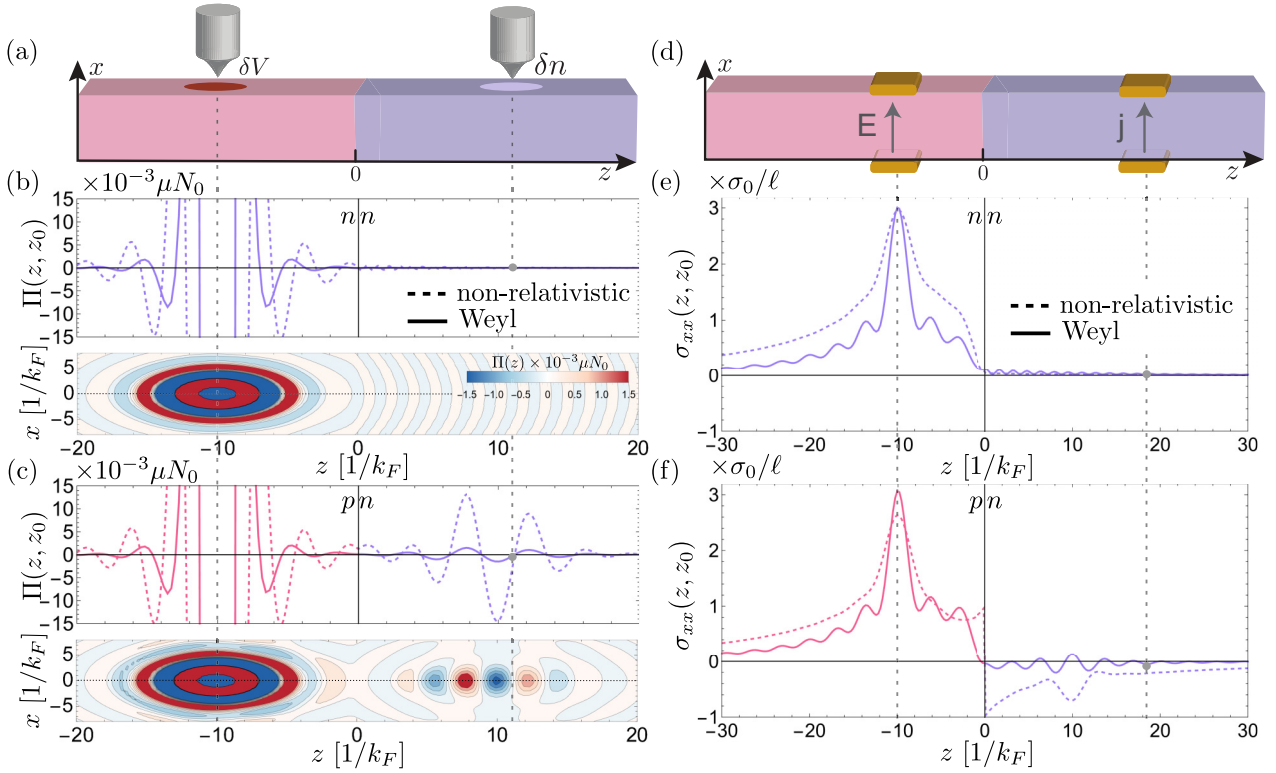
FIG. 2. Veselago lensing of a single chirality in spectroscopy and nonlocal transport. (a) Schematic setup to measure Veselago lensing spectroscopically (see Supplemental Material [25] for a two-chirality setup). (b) The upper plot shows the nonlocal polarizability $\Pi(z, z')$ for an n-n junction as a function of z for $(x, y) = (0, 0)$ for both nonrelativistic (dashed) and Weyl band structures (solid). The contour plot shows $\Pi(z, z')$ in the (x, z) plane for $y = 0$ for the Weyl case. (c) Same as (b) for a p-n junction. In (b) and (c) $\Pi(z, z')$ is given in units of μN_0, with $N_0 = k_F^3/(2\pi^2\mu_L)$ the density of states on the left of the junction. (d) Schematic setup to measure Veselago lensing in nonlocal transport (see Supplemental Material [25] for a two-chirality setup). (e) and (f) show the nonlocal conductivity $\sigma_{xx}(z, z')$ for n-n and p-n junctions, respectively. (b) and (e) are calculated with $(m, \mu, \ell)_L = (1, 0.5, 50)$ and $(v, \mu, \ell)_R = (2, 4, 50)$ for the nonrelativistic case, and $(v, \mu, \ell)_L = (1, 1, 50)$ and $(v, \mu, \ell)_R = (1, 2, 50)$ for the Weyl case. (c) and (f) are calculated with $(m, \mu, \ell)_L = (1, 0.5, 50)$ and $(v, \mu, \ell)_R = (-1, -0.5, 50)$ for the nonrelativistic case, and $(v, \mu, \ell)_L = (1, 1, 50)$ and $(v, \mu, \ell)_R = (1, -1, 50)$ for the Weyl case. In (e) and (f) the conductivity is given in units of the total conductivity σ_0 over the mean free path ℓ (see Supplemental Material [25]).

3D electron gases because finding junctions with equal k_F but opposite carrier types is challenging in practice. Later we will argue how the chiral anomaly of a 3D Weyl semimetal aids to tune into this ideal condition by varying the magnetic field.

IV. NONLOCAL TRANSPORT IN A CHIRAL VESELAGO LENS

While the image charge is convenient to understand how Veselago lensing can be enhanced (see Supplemental Material [25] for a proposed device), surface state contributions must be factored out [32–35] to reveal Veselago lensing. A bulk, nonlocal transport measurement, such as that depicted in Fig. 2(d), is in this sense a simpler setup. In a local electric field $\mathbf{E}(z) = \mathbf{E}_0\delta(z - z_0)$ the electronic current $j_\mu(z) = \sigma_{\mu\nu}(z, z_0)E_\nu$ is obtained from the nonlocal conductivity [36,37]

$$\sigma_{\mu\nu}(z, z') = \int \frac{dS_z dS_{z'}}{\pi \mathcal{A}} \text{Tr}\big[\hat{j}_\mu \, \text{Im} \, \hat{G}(z, z')\hat{j}_\nu \, \text{Im} \, \hat{G}(z, z')\big], \quad (4)$$

where $\hat{j}_\mu$ are the components of the current operator, with $\mu = x, y, z$, and S_z and $S_{z'}$ are planes at z and z' with areas $\mathcal{A}$. The nonlocal conductivity is a complex quantity that accounts

for the dephasing between the two probes. In Eq. (4) we only show its real part, which can be measured by averaging the conductivities obtained after permuting the positions z and z' of the leads (see Supplemental Material [25]).

In Figs. 2(e) and 2(f), we show the nonlocal conductivity for an n-n (or p-p) and an n-p junction. For an n-n junction, the current is positive and decays exponentially away from the input electric field, as shown in Fig. 2(e). In contrast, for the p-n junction, the current changes sign when crossing the interface and its magnitude peaks close to the image charge, signaling the presence of a Veselago lens [38]. Note that the negative current does not violate energy conservation, since the total current is positive, and is a consequence of the change of the type of the main carriers.

As with the image Veselago charge, the image Veselago current is larger for a 3D electron gas than for a Weyl semimetal, where it oscillates close to zero, but negative on average. These oscillations are absent in the 3D electron gas which is a single-band model, and thus we attribute them to interband excitations that lead to holelike and electronlike regions. Lastly, we find that ideal lensing is achieved when both sides of the p-n junction are tuned to have the same k_F, as for the image Veselago charge.
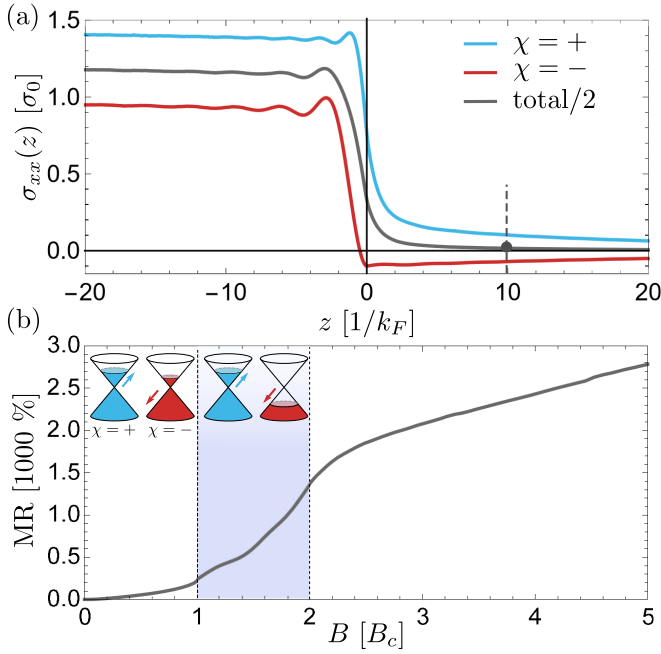
FIG. 3. Transport signatures of the chiral Veselago lens depicted in Fig. 1. (a) The total nonlocal conductivity $\sigma_{xx}(z)$ (dark curve) for $B = 2B_c$. The contribution of each chirality is plotted as colored curves. $\sigma_{xx}(z)$ is uniform for $z < 0$ where the electric field is constant and drops for $z > 0$, with a negative conductivity for Weyl quasiparticles with chirality $\chi = -$. (b) Giant magnetoresistance due to the chiral anomaly for a probe located at $z = 10/k_F$; see the dashed line in (a). The magnetic field is in units of $B_c = 2\mu^3/(3v^3 e^2 \tau E) \approx 1T$ (see text). Chiral Veselago lensing starts at $B = B_c$, which marks the change from electrons to holes for chirality $\chi = -$ (inset red cone). For $B > B_c$ carriers with $\chi = -$ contribute with a negative current that is maximal at $B = 2B_c$, when the Fermi wave vector is opposite of both sides of the junction. The strong increase in magnetoresistance, marked by the blue region, is thus a fingerprint of chiral Veselago lensing.

V. SIGNATURES OF A 3D CHIRAL VESELAGO LENS

We have previously considered the transport of each chirality individually, while in the setup of Fig. 1, the two chiralities are present. In this setup the electric field E is finite for $z < 0$, and zero for $z > 0$. In Fig. 3(a) we show the resulting total nonlocal conductivity and the contribution of each chirality, calculated using the expression

$$\sigma_{xx}(z) = \int_{-\infty}^{0} dz' \, \sigma_{xx}(z, z'). \tag{5}$$

For $z > 0$, $\sigma_{xx}(z)$ decays slowly and the contribution of each chirality is about 10% of the bulk conductivity at $zk_F = 10$. Since the conductivity is negative for one chirality and positive for the other, the two contributions compensate and lead to a giant magnetoresistance with respect to the configuration without chiral anomaly. This follows from our previous discussion: Because of the chiral anomaly, carriers of one chirality (here, $\chi = -$) experience a p-n junction while carriers of the opposite chirality (here, $\chi = +$) experience an n-n junction. Since E extends for all $z < 0$, the p-n junction

leads to an extended, rather than localized, Veselago image. Nonetheless, the ideal condition for an optimal image is still $k_{F,L} = k_{F,R}$. Accordingly, we find that the negative current is maximal when this condition is met.

The total $\sigma_{xx}(z)$ of the junction is a sum of the contributions of each Weyl cone. As seen in Fig. 3(a), the total $\sigma_{xx}(z)$ is positive throughout the junction (dark curve), since the total charge is conserved, hiding the signature of Veselago lensing. However, Veselago lensing becomes apparent when studying the nonlocal resistivity as a function of B, as shown in Fig. 3(b). At $B < B_c$ there is no chiral Veselago lensing and the magnetoresistance increases moderately. This is due to the increasing mismatch between the carrier densities on each side of the junction. Once $B > B_c$, an effective p-n junction is formed for one chirality (here, $\chi = -$) that leads to a negative contribution to current and thus to a giant increase in the magnetoresistivity [shaded region in Fig. 3(b)]. The amplitude of the negative current is maximal at $B = 2B_c$ where $k_{F,L} = k_{F,R}$ for $\chi = -$, and Veselago lensing is optimal. For $B > 2B_c$ the amplitude of the negative current decreases, and the magnetoresistance increases moderately. The strong increase in magnetoresistance within $[B_c, 2B_c]$, highlighted in Fig. 3(b), is thus a fingerprint of chiral Veselago lensing.

VI. DISCUSSION

We have determined how the chiral anomaly of Weyl semimetals can be used to create a Veselago lens that distinguishes electrons by their chirality. We have uncovered that the chiral Veselago lens based on Weyl semimetals is advantageous for several reasons. First, a chiral Veselago lens eliminates the charge buildup at the interface, since it requires a single material, and the total charge remains constant along the sample. Second, the chiral anomaly allows one to control the k_F of each chirality using a magnetic field. This allows one to detect chiral Veselago lensing by measuring nonlocal conductivity and tune it to the ideal condition for lensing. This property goes beyond current graphene-based proposals, since the chiral anomaly is unique to 3D Weyl semimetals.

We have neglected several effects in our computations. First, we neglected the orbital localization in a magnetic field, since this occurs over the magnetic length scale $\ell_B \approx 25.6$ nm$/\sqrt{B[\text{T}]} \gg z, \lambda_F$. Second, tilted Weyl cones [20] could prevent a perfect matching of k_F. However, the chiral anomaly is often observed in systems where the Weyl cones are generated by magnetic field from a lightly doped semimetal, e.g., GdPtBi, ZrTe$_5$, or KZnBi [17,39–41], where the effect of tilting is negligible. Lastly, Fermi arcs will be negligible in nonlocal transport, as it is a bulk probe.

The estimates we provide indicate that chiral Veselago lensing is observable under moderate electric and magnetic fields. Nonlocal transport experiments have probed the chiral anomaly, albeit without p-n-junctions and lensing [22,42], suggesting that our proposal can be realized using current technology. Our work opens the possibility to realize a device that can control a computational degree of freedom using Veselago lensing in 3D materials, enabled by the chiral anomaly.

[1] C. Yan, M. Pepper, P. See, I. Farrer, D. Ritchie, and J. Griffiths, Sci. Rep. **10**, 2593 (2020).

[2] J. Spector, H. L. Stormer, K. W. Baldwin, L. N. Pfeiffer, and K. W. West, Appl. Phys. Lett. **56**, 1290 (1990).

[3] V. V. Cheianov, V. Fal'ko, and B. L. Altshuler, Science **315**, 1252 (2007).

[4] A. Weststrom and T. Ojanen, Phys. Rev. X **7**, 041026 (2017).

[5] M. Karalic, A. Štrkalj, M. Masseroni, W. Chen, C. Mittag, T. Tschirky, W. Wegscheider, T. Ihn, K. Ensslin, and O. Zilberberg, Phys. Rev. X **10**, 031007 (2020).

[6] V. Veselago, Sov. Phys. Usp. **10**, 509 (1968).

[7] R. D. Y. Hills, A. Kusmartseva, and F. V. Kusmartsev, Phys. Rev. B **95**, 214103 (2017).

[8] F. Libisch, T. Hisch, R. Glattauer, L. A. Chizhova, and J. Burgdörfer, J. Phys.: Condens. Matter **29**, 114002 (2017).

[9] H. Tian and J. Wang, J. Phys.: Condens. Matter **29**, 385401 (2017).

[10] S.-H. Zhang, J.-J. Zhu, W. Yang, and K. Chang, 2D Mater. **4**, 035005 (2017).

[11] S.-H. Zhang and W. Yang, New J. Phys. **21**, 103052 (2019).

[12] Y. Yang, Y. Bi, L. Peng, B. Yang, S. Ma, H.-C. Chan, Y. Xiang, and S. Zhang, Optica **8**, 249 (2021).

[13] G.-H. Lee, G.-H. Park, and H.-J. Lee, Nat. Phys. **11**, 925 (2015).

[14] S. Chen, Z. Han, M. M. Elahi, K. M. M. Habib, L. Wang, B. Wen, Y. Gao, T. Taniguchi, K. Watanabe, J. Hone, A. W. Ghosh, and C. R. Dean, Science **353**, 1522 (2016).

[15] X. Zhang, W. Ren, E. Bell, Z. Zhu, K. Watanabe, T. Taniguchi, E. Kaxiras, M. Luskin, and K. Wang, arXiv:2106.09651.

[16] B. Brun, N. Moreau, S. Somanchi, V.-H. Nguyen, K. Watanabe, T. Taniguchi, J.-C. Charlier, C. Stampfer, and B. Hackens, Phys. Rev. B **100**, 041401(R) (2019).

[17] N. P. Armitage, E. J. Mele, and A. Vishwanath, Rev. Mod. Phys. **90**, 15001 (2018).

[18] Z. Zhang and J. T. Yates, Chem. Rev. **112**, 5520 (2012).

[19] D. E. Kharzeev and Q. Li, arXiv:1903.07133.

[20] A. A. Soluyanov, D. Gresch, Z. Wang, Q. Wu, M. Troyer, X. Dai, and B. A. Bernevig, Nature (London) **527**, 495 (2015).

[21] K. Landsteiner, Acta Phys. Pol., B **47**, 2617 (2016).

[22] S. A. Parameswaran, T. Grover, D. A. Abanin, D. A. Pesin, and A. Vishwanath, Phys. Rev. X **4**, 031035 (2014).

[23] J. Behrends, A. G. Grushin, T. Ojanen, and J. H. Bardarson, Phys. Rev. B **93**, 075114 (2016).

[24] P. E. C. Ashby and J. P. Carbotte, Phys. Rev. B **89**, 245121 (2014).

[25] See Supplemental Material at http://link.aps.org/supplemental/10.1103/PhysRevB.105.075309 for the detailed calculation of the Green's functions of a junction of a 3D electron gas and of a Weyl semimetal, detailed calculations of the bulk nonlocal conductivity of a Weyl semimetal and figures to illustrate how Veselago lensing is affected by a smooth junction and to changes in the carrier densities, and two additional device proposals to detect the chiral Veselago lensing, one using an STM, and another using nonlocal transport, which includes Refs. [43–45].

[26] G. Giuliani and G. Vignale, *Quantum Theory of the Electron Liquid* (Cambridge University Press, Cambridge, UK, 2005).

[27] H.-R. Chang, J. Zhou, S.-X. Wang, W.-Y. Shan, and D. Xiao, Phys. Rev. B **92**, 241103(R) (2015).

[28] M. V. Hosseini and M. Askari, Phys. Rev. B **92**, 224435 (2015).

[29] V. Kaladzhyan, A. A. Zyuzin, and P. Simon, Phys. Rev. B **99**, 165302 (2019).

[30] L. J. Godbout, S. Tchoumakov, and W. Witczak-Krempa, Phys. Rev. B **102**, 205202 (2020).

[31] R. Pierret, *Semiconductor Device Fundamentals* (Addison-Wesley, Boston, 1996), pp. 200–234.

[32] H. Inoue, A. Gyenis, Z. Wang, J. Li, S. W. Oh, S. Jiang, N. Ni, B. A. Bernevig, and A. Yazdani, Science **351**, 1184 (2016).

[33] R. Batabyal, N. Morali, N. Avraham, Y. Sun, M. Schmidt, C. Felser, A. Stern, B. Yan, and H. Beidenkopf, Sci. Adv. **2**, 1600709 (2016).

[34] S. Kourtis, J. Li, Z. Wang, A. Yazdani, and B. A. Bernevig, Phys. Rev. B **93**, 041109(R) (2016).

[35] Q.-Q. Yuan, L. Zhou, Z.-C. Rao, S. Tian, W.-M. Zhao, C.-L. Xue, Y. Liu, T. Zhang, C.-Y. Tang, Z.-Q. Shi, Z.-Y. Jia, H. Weng, H. Ding, Y.-J. Sun, H. Lei, and S.-C. Li, Sci. Adv. **5**, eaaw9485 (2019).

[36] X.-G. Zhang and W. H. Butler, Phys. Rev. B **51**, 10085 (1995).

[37] H. U. Baranger and A. D. Stone, Phys. Rev. B **40**, 8169 (1989).

[38] S. W. LaGasse and C. D. Cress, Nano Lett. **20**, 6623 (2020).

[39] J. Cano, B. Bradlyn, Z. Wang, M. Hirschberger, N. P. Ong, and B. A. Bernevig, Phys. Rev. B **95**, 161306(R) (2017).

[40] J. Song, S. Kim, Y. Kim, H. Fu, J. Koo, Z. Wang, G. Lee, J. Lee, S. H. Oh, J. Bang, T. Matsushita, N. Wada, H. Ikegami, J. D. Denlinger, Y. H. Lee, B. Yan, Y. Kim, and S. W. Kim, Phys. Rev. X **11**, 021065 (2021).

[41] Z. Wang, Y. Sun, X.-Q. Chen, C. Franchini, G. Xu, H. Weng, X. Dai, and Z. Fang, Phys. Rev. B **85**, 195320 (2012).

[42] C. Zhang, E. Zhang, W. Wang, Y. Liu, Z.-G. Chen, S. Lu, S. Liang, J. Cao, X. Yuan, L. Tang, Q. Li, C. Zhou, T. Gu, Y. Wu, J. Zou, and F. Xiu, Nat. Commun. **8**, 13741 (2017).

[43] R. A. Morrow, Phys. Rev. B **35**, 8074 (1987).

[44] G. T. Einevoll and P. C. Hemmer, J. Phys. C: Solid State Phys. **21**, L1193 (1988).

[45] D. Pfirsch and R. N. Sudan, J. Math. Phys. **32**, 1774 (1991).